orient by 60° jumps, e.g., a defect with a [110] $\hat{r}_1$ orientation can only jump to $\hat{r}_3$, $\hat{r}_4$, $\hat{r}_5$, and $\hat{r}_6$ orientations. As mentioned earlier the good agreement between the absorption coefficient ratios predicted from the polarized luminescence measurements and those values actually observed, as given in Table IV, indicates that the emission is due to F_2 centers and that it is primarily a σ-σ transition.

Dreyfus[9] and Schneider[10] have investigated the reorientation of F_A centers and F_2 centers, respectively. Schneider found that F_2 centers reorient indirectly by the formation of F_2^+ centers which then absorb light and rotate. When the reoriented F_2^+ centers capture electrons then reoriented F_2 centers are formed. F_2^+ centers have not yet been observed in $KMgF_3$; however, our data are not inconsistent with this interpretation.

In summary it has been shown that F_2 centers have absorption transitions at 282- and 445-nm and an emission at 590 nm. F_3 centers absorb light of 250 and 396 nm and emit light of 465 nm. Both of these color centers can be reoriented by polarized bleaching light, but the exact mechanism for this reorientation is not yet known.

†This research was supported by the U. S. AEC under contract with Union Carbide Corp., by AEC equipment Grant No. AT-(40-1)-4080, and by the National Science Foundation.

*Present address: Spin-Labs, Knoxville, Tenn.

[1]T. P. P. Hall, Brit. J. Appl. Phys. 17, 1011 (1966).

[2]T. P. P. Hall and A. Leggeat, Solid State Commun. 7, 1651 (1969).

[3]C. R. Riley and W. A. Sibley, Phys. Rev. B 1, 2789 (1970).

[4]T. L. Lewis, J. L. Kolopus, and E. Sonder (unpublished).

[5]C. R. Riley, Ph. D. thesis (University of Tennessee, 1970) (unpublished).

[6]P. P. Feofilov, *The Physical Basis of Polarized Emission* (Consultants Bureau, New York, 1961).

[7]J. J. Markham, in *Solid State Physics*, edited by F. Seitz and D. Turnbull (Academic, New York, 1966), Suppl. 8; Rev. Mod. Phys. 31, 956 (1959).

[8]D. B. Fitchen, in *The Physics of Color Centers*, edited by W. B. Fowler (Academic, New York, 1968).

[9]R. W. Dreyfus, Phys. Rev. B 1, 4826 (1970).

[10]I. Schneider, Phys. Rev. Letters 24, 1296 (1970).

PHYSICAL REVIEW B VOLUME 5, NUMBER 8 15 APRIL 1972

Ultrasonic Propagation, Stress Effects, and Interaction Parameters at the Displacive Transition in $SrTiO_3$

K. Fossheim

Department of Physics, University of Trondheim, Norges Tekniske Høgskole, Trondheim, Norway

and

B. Berre*

Department of Physics, University of Oslo, Oslo, Norway

(Received 16 September 1971)

The interaction between strain and order parameter at the structural transition in $SrTiO_3$ is investigated by ultrasonic measurements of attenuation, velocity shifts, and stress dependence of the transition temperature T_a. A method is described by which measurements of domain attenuation are used to correct the velocity data below T_a. Also, biaxial pressure has been successfully used to suppress the domain structure in the tetragonal phase. By comparing the experimental results with the consequences of a phenomenological configurational potential the interaction parameters are deduced. The model is found to correlate the experimental results in a consistent way. The hydrostatic-pressure dependence of T_a is predicted to be $dT_a/dp = 0.5 \times 10^{-3}$ K/dyn cm^{-2}. Critical effects in sound velocity and attenuation are briefly described.

I. INTRODUCTION

During the past few years the compound $SrTiO_3$ has attracted increasing attention from different branches of solid-state physics. The primary reason for the interest in this material is the fact that its structural transition is associated with a condensation of a (triply degenerate) lattice mode, often referred to as a soft mode. $SrTiO_3$ has, in fact, become a major testing ground for the soft-mode theory of solid-state transitions.[1] Furthermore, $SrTiO_3$ belongs to a family of perovskite-type compounds—including, for instance, $KMnF_3$, $LaAlO_3$, and $CsPbCl_3$—possessing cubic symmetry in the high-temperature phase ($T > T_a$). In the low-temperature phase ($T < T_a$) different symmetries are

found, all connected with relatively small cooperative static displacements of the atomic arrangement from cubic structure.

In the present paper we continue the discussion[2,3] of ultrasonic propagation in $SrTiO_3$. The main emphasis will be on the information that can be gained about the interaction between strain and order parameter. The experiments related to this problem include measurement of (a) attenuation as a function of temperature, frequency, and pressure; (b) the dependence of the transition temperature upon uniaxial and biaxial (planar) stress; and (c) sound velocities under various stress conditions. In order to extract the expansion parameters and to test the consistency of the results it is necessary to discuss the theory in some detail with regard to both monodomain and multidomain behavior. The experimental technique was designed to reveal the domain influence which has not previously been studied systematically by other authors. It is demonstrated how the domain formation can be effectively prevented by applying suitable stress.

The theoretical discussion is confined to Sec. II. Section III contains a short description of some experimental details. The presentation of results is given in Sec. IV, followed by a discussion in Sec. V.

In addition to experiments which could be discussed in fairly simple terms by use of the energy expansion mentioned above, the present research has, since the beginning,[2] been aimed at a study of the complex questions associated with the nature of the transition: Is it a continuous phase change? What kind of singularities appear at the transition?

In Ref. 2 it was pointed out that the transition was continuous at least to within a few hundredths of a degree. In this respect $SrTiO_3$ represents a rather rare case among structural transitions. In recent years experimental as well as theoretical evidence has pointed towards a number of common features in continuous transitions—be it transitions between solid phases or others. Concepts like scaling and universality reflect most strongly the belief in these inherent similarities. Hopefully such hypotheses may also be put to a test in $SrTiO_3$. Previous[2] and present results (Sec. IV) indicate that such tests should be possible to make when truly high-quality samples can be obtained. At the present time we have found it possible to deduce (Sec. IV) the temperature exponents for attenuation below as well as above T_a, and to answer the question whether critical scattering takes place, in addition to Landau-Khalatnikov (LK) dispersion.

II. THEORY

Although it had long ago been realized by Müller[4] that a static rotation of the oxygen octahedra might be involved in the structural change taking place in $SrTiO_3$ at $T_a \approx 106$ K, it was not until the EPR measurements of Unoki and Sakudo[5] and of Müller *et al.*,[6] and the Raman work of Fleury *et al.*,[7] that the full role of these octahedra was appreciated. It could be concluded that the R-corner optic mode is a temperature-dependent mode going "soft" at the transition.

When expanding the configurational energy of $SrTiO_3$ in Landau form it is generally necessary to introduce three order parameters corresponding to the possible rotation of oxygen octahedra around each cube axis. However, when considering only static or quasistatic effects in the tetragonal low-temperature phase, one order parameter is sufficient. We shall confine most of our attention to this simpler case and give the corresponding energy expression as derived from those of Slonczewski and Thomas[8] and Slonczewski,[9] which are refined and extended versions of the model potential used by Thomas and Müller.[10] Our simplified expression is then

$$U = U_0 + \tfrac{1}{2}KQ^2 + AQ^4 - [B_1 e_3 + B_2(e_1+e_2)]Q^2 + \tfrac{1}{2}C_{11}(e_1^2+e_2^2+e_3^2) + C_{12}(e_1e_2+e_2e_3+e_3e_1) + \tfrac{1}{2}C_{44}(e_4^2+e_5^2+e_6^2) - \sum e_i T_i \,. \quad (1)$$

Strain notation is here as follows:

$$e_{ii} = e_i = \frac{\partial u_i}{\partial x_i}, \quad i = 1, 2, 3,$$

$$e_{23} = e_4 = \frac{\partial u_2}{\partial x_3} + \frac{\partial u_3}{\partial x_2}, \text{ etc.},$$

where u_j are the displacements and the x_i the coordinates. The z axis ($i = 3$) has been chosen along the tetragonal c axis so that $\vec{Q} = Q(0, 0, 1)$. Equation (1) will be recognized as a simple Landau expansion with Q proportional to the order parameter and with additional terms corresponding to interaction between order parameter and elastic strain, elastic-energy terms, and interaction between applied stress T_i and elastic strain. Since we do not consider order-parameter fluctuations or other forms of inhomogeneities from a theoretical point of view the gradient term in the Landau expansion is omitted. U_0 contains the transition-independent terms.

In Refs. 8 and 9 the interaction with volume strain was neglected by putting $B_1 = -2B_2$. This approximation will not be made here, since we are interested in the stress dependence of the transition temperature, and neglect of volume-strain interaction makes T_a independent of hydrostatic pressure. Thermal expansion would also be unaffected by the transition in such an approximation. Since measurements of both types[11,12] have been done, and nonvanishing effects have been found, we find it worthwhile to pursue this point. It is also relevant to the experimental results presented here (Secs. IV and V).

A. Spontaneous Strain and Interaction Parameters B_1 and B_2

The set of equations that will give the equilibrium values of e_i in terms of Q is obtained by setting $\partial U/\partial e_i = 0$. We find

$$\begin{aligned} &C_{11}e_1 + C_{12}e_2 + C_{12}e_3 = B_2 Q^2 + T_1 , \\ &C_{12}e_1 + C_{11}e_2 + C_{12}e_3 = B_2 Q^2 + T_2 , \\ &C_{12}e_1 + C_{12}e_2 + C_{11}e_3 = B_1 Q^2 + T_3 , \\ &C_{44}e_4 = T_4 ; \quad C_{44}e_5 = T_5 ; \quad C_{44}e_6 = T_6 . \end{aligned} \tag{2}$$

The resulting elastic strains are

$$\begin{aligned} e_1 &= \frac{1}{3BC_e}[(C_{11}B_2 - C_{12}B_1)Q^2 + 3BT_1 \\ &\quad - C_{12}(T_1 + T_2 + T_3)] , \\ e_2 &= \frac{1}{3BC_e}[(C_{11}B_2 - C_{12}B_1)Q^2 + 3BT_2 \\ &\quad - C_{12}(T_1 + T_2 + T_3)] , \\ e_3 &= -\frac{1}{3BC_e}\left\{[2C_{12}B_2 - (C_{11} + C_{12})B_1]Q^2 \right. \\ &\quad \left. + C_{12}\left[T_1 + T_2 - \left(1 + \frac{C_{11}}{C_{12}}\right)T_3\right]\right\} , \end{aligned} \tag{3}$$

with

$$C_e \equiv C_{11} - C_{12} , \quad 3B \equiv (C_{11} + 2C_{12}) .$$

Furthermore it is seen that

$$e_3 - e_1 = \frac{1}{C_e}(B_1 - B_2)Q^2 + \frac{1}{C_e}(T_3 - T_1) . \tag{4}$$

At $T_i = 0$ one has a simple expression for the difference between the interaction parameters in terms of measureable quantities;

$$B_1 - B_2 = C_e[(e_3 - e_1)/Q^2] . \tag{5}$$

Q is related to the static rotation angle of the oxygen octahedra by $\tan\phi = 2Q/a_0$, where a_0 is the lattice constant. Taking the ratio of spontaneous strains we find

$$\frac{e_1}{e_3} = -\frac{\mu_c - \mu_b}{1 + \mu_c - 2\mu_c\mu_b} , \tag{6}$$

with $\mu_c \equiv C_{12}/C_{11}$; $\mu_b \equiv B_2/B_1$. The ratio of the coupling coefficients is therefore

$$\frac{B_2}{B_1} = \mu_b = \frac{\mu_c + (1 + \mu_c)(e_1/e_3)}{1 + 2\mu_c(e_1/e_3)} . \tag{7}$$

The measurements that are needed to determine $B_1 - B_2$ also determine B_2/B_1, and thus B_1 and B_2 individually.

B. Stress Dependence of T_a, and Coupling Parameters B_1 and B_2

Another type of experiment which can be performed to determine B_1 and B_2 is the measurement of the dependence of the transition temperature T_a on uniaxial, biaxial, or hydrostatic stress.

Inserting the strains Eq. (3) in the energy expression Eq. (1) and collecting terms of second order in Q, the transition temperature is defined as that temperature which makes the coefficient vanish.

Introducing pressure variables $p_i = -T_i$ and taking the derivative of the Q^2 coefficient with respect to p_i, the result for a pressure p_1 is

$$\frac{dT_a}{dp_1} = \frac{4}{3BC_e}\left(1\Big/\frac{dK}{dT}\right)(C_{12}B_1 - C_{11}B_2) \tag{8a}$$

when K is a function of $T - T_a$. We note that Eq. (8a) may be written as

$$\frac{dT_a}{dp_1} = -\left(4\Big/\frac{dK}{dT}\right)\frac{e_1(0)}{Q^2} , \tag{8b}$$

where $e_1(0)$ is the temperature-dependent (spontaneous) strain e_1 at zero stress.

Similarly, we find with pressure p_3 along the c axis and with hydrostatic pressure p

$$\begin{aligned} \frac{dT_a}{dp_3} &= -\left(4\Big/3BC_e\frac{dK}{dT}\right)[(C_{11} + C_{12})B_1 - 2C_{12}B_2] \\ &= -\left(4\Big/\frac{dK}{dT}\right)\frac{e_3(0)}{Q^2} , \\ \frac{dT_a}{dp} &= -\left(4\Big/3B\,\frac{dK}{dT}\right)(B_1 + 2B_2) \\ &= -\left(4\Big/\frac{dK}{dT}\right)\frac{e_1(0) + e_2(0) + e_3(0)}{Q^2} . \end{aligned} \tag{8c}$$

We note that Slonczewski's Eq. (A5) for dT_a/dp_3 contains $e_3(0) - e_1(0)$ instead of just $e_3(0)$. This illustrates a shortcoming of the assumption $B_1 = -2B_2$.

Taking the ratios between pressure dependences given in Eqs. (8a)–(8c), we obtain

$$\begin{aligned} \frac{dT_a}{dp}\Big/\frac{dT_a}{dp_1} \equiv \kappa_1 &= -C_e\frac{B_1 + 2B_2}{C_{12}B_1 - C_{11}B_2} \\ &= -\frac{(1 - \mu_c)(1 + 2\mu_b)}{\mu_c - \mu_b} , \end{aligned} \tag{9a}$$

which means that the measurements of uniaxial and hydrostatic stress dependences determine the ratio μ_b once μ_c is known. The inverted relation is also useful:

$$\frac{B_2}{B_1} = \mu_b = -\frac{1 - \mu_c + \mu_c\kappa_1}{2 - 2\mu_c - \kappa_1} . \tag{9b}$$

Similarly,

$$\begin{aligned} \frac{dT_a}{dp}\Big/\frac{dT_a}{dp_3} \equiv \kappa_3 &= C_e\frac{B_1 + 2B_2}{(C_{11} + C_{12})B_1 - 2C_{12}B_2} \\ &= \frac{(1 - \mu_c)(1 + 2\mu_b)}{1 + \mu_c - 2\mu_c\mu_b} , \end{aligned} \tag{10a}$$

which means that

$$\frac{B_2}{B_1}=\mu_b=\frac{1-\mu_c-(1+\mu_c)\kappa_3}{2\mu_c(1-\kappa_3)-2}\,. \tag{10b}$$

The ratio between uniaxial-stress dependences is

$$\frac{dT_a}{dp_1}\Big/\frac{dT_a}{dp_3}\equiv\kappa_{13}=-\frac{C_{12}B_1-C_{11}B_2}{(C_{11}+C_{12})B_1-2C_{12}B_2}$$

$$=-\frac{\mu_c-\mu_b}{1+\mu_c-2\mu_c\mu_a}\,. \tag{10c}$$

The following relations are particularly simple:

$$\kappa_1=\frac{e_1(0)+e_2(0)+e_3(0)}{e_1(0)}\,,$$

$$\kappa_3=\frac{e_1(0)+e_2(0)+e_3(0)}{e_3(0)}\,, \tag{11}$$

$$\kappa_{13}=\frac{e_1(0)}{e_3(0)}\,.$$

In other words the ratios between various derivatives of T_a with respect to pressure are simply equal to the ratios between corresponding components of spontaneous strain.

Finally, the difference B_1-B_2 is given by

$$B_1-B_2=-\tfrac{1}{4}C_e\left(\frac{dK}{dT}\right)\left(\frac{dT_a}{dp_3}-\frac{dT_a}{dp_1}\right). \tag{12}$$

At this point we would like to make a comment regarding the expansion used in the foregoing. As recent experiments[2,3,13,14] have shown, Landau theory is incorrect in a range of a few degrees above and below T_a. Still, the Landau form is exactly what we have used. We do not believe, however, that this imposes serious limitations on the validity of the expressions we have given. The reasoning which leads to such a conclusion is the following.

We regard, in principle, the energy expansion employed as an expansion not around T_a, the actual transition temperature, but rather around T_a', the temperature towards which the experimental results for Q^2 in the subcritical region extrapolate[13,14] (see Fig. 1). As a consequence of this reasoning we must regard the calculations of the stress dependence of the transition temperature given above as, strictly speaking, a calculation of the stress dependence of T_a'. However, we see no reason why dT_a/dp, etc., should be much different from dT_a'/dp, etc. The simplest argument leading to this conclusion is the following: In analogy with the situation in superconductors[15] one may expect that the reason why the transition occurs at T_a instead of T_a' is to be found in the fluctuations of the system; the transition temperature is renormalized as a consequence of the interaction between fluctuations. In $SrTiO_3$ this renormalization is about 5%. Putting on a relatively low pressure will not change the fluctuations when measured on a temperature scale with $T_a(p)$ as origin. Nor can it then to first order change the amount of depression of $T_a(p)$ below $T_a'(p)$ since the depression is caused by exactly these fluctuations. Thus we conclude that dT_a/dp, etc., equals dT_a'/dp, etc., to a good approximation, and the use of the Landau form in the foregoing therefore appears justified. All measurements used in determining the interaction parameters must, of course, be performed outside the critical region, since this is where the Landau form may be assumed valid.

Feder and Pytte[16–18] have taken a step beyond the Landau expansion and developed a microscopic theory based on a model Hamiltonian and including correlations. In this way they were able to *determine* the temperature dependences of the soft modes and the order parameter through a derivation of the correlation functions. Still, the results are mostly within the mean-field category, and as such in substantial agreement with the consequences of the Landau expansion. Analysis of the theory of Feder and Pytte shows, in fact, that exactly the same set of equations as given above may be deduced from their model Hamiltonian in the mean-field limit.

C. Elastic Constants and Coupling Parameters B_1 and B_2

The elastic constants in the tetragonal phase C_{ij}^t are readily obtained from the full energy expres-

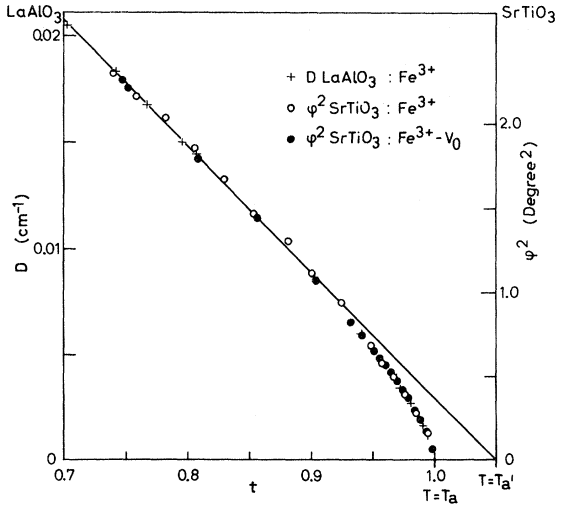

FIG. 1. Adapted from Ref. 13, showing the crystalline field parameter D in $LaAlO_3$ and the rotational angle ϕ in $SrTiO_3$ as functions of reduced temperature $t=T/T_a$. Deviation from the straight line is interpreted in Ref. 13 as changeover from Landau behavior to critical behavior. T_a' is the point where the extrapolated line meets the t axis.

sion[10]:

$$C_{11}^t = C_{11} - B_2^2 F_3\,,\quad C_{33}^t = C_{11} - B_1^2 F_3\,,\quad C_{12}^t = C_{12} - B_2^2 F_3\,,$$
$$C_{13}^t = C_{13} - B_1 B_2 F_3\,,\quad C_{44}^t = C_{44} - B_t^2 F_{1,2}\,,\quad C_{66}^t = C_{44}\,, \tag{13}$$

where coefficients C_{ij} without superscript refer to the cubic phase. The parameters $F_{1,2}$ and F_3 are defined by

$$F_{1,2} = Q^2/\rho_r\,\omega_{1,2}^2\,,\quad F_3 = 4Q^2/\rho_r\,\omega_3^2\,, \tag{14}$$

where ρ_r is the mass density associated with the rotating atoms of the oxygen octahedra when rotation is about a cube axis, $\omega_{1,2}$ and ω_3 are, respectively, the degenerate and nondegenerate soft-mode frequencies below T_a, and B_t is the parameter describing coupling between rotational strains and pairs of orthogonal oxygen displacements. [The corresponding term in the energy expansion is not included in Eq. (1).] Ultrasonic velocity measurements, in principle, establish the quantities ΔC_{ij}. For the determination of Q^2 and the soft-mode frequencies $\omega_{1,2}^2$ and ω_3^2 other types of measurements must be performed. In practice, therefore, velocity measurements may be said to establish the interaction constants B_1, B_2, and B_t. When coupling to volume strain is retained, $\omega_{1,2}$ and ω_3 are rather complicated functions of the coefficients in the full energy expansion, but we prefer to regard them here as quantities which can be found experimentally from Raman and neutron measurements. Pytte[19] has discussed in more detail the behavior of elastic constants in the transition region.

D. Sound Velocity below T_a

The difficulties encountered in measurements of sound velocity below the transition temperature are best illustrated by the somewhat diverse results[12,20–24] obtained. These difficulties are primarily due to the domain formation which occurs below T_a. The additional anisotropy caused by the domains, together with domain wall motion which must occur under influence of an elastic wave, make important contributions to the effective elastic constants. In none of the ultrasonic investigations of Refs. 12, 23, and 24 have corrections been made for the interaction with domain walls below T_a.

We shall discuss two ways of solving this difficulty experimentally. First of all one has the option of applying stress in such a way that the domain structure is suppressed and a monodomain tetragonal phase produced (see Sec. IV). Second, one may calculate the domain contribution to the total velocity change from attenuation data. Neither method has been tried by previous workers. The second alternative requires some comments.

In order to extract the elastic constants from velocity measurements in a domain structure, two things need to be done: One has to express the averaged elastic constants in terms of the individual elastic constants, and to calculate correction terms due to domain wall motion. To execute the averaging properly, knowledge of the complete distribution of domains and c axes is required. This kind of information is, of course, not available, so one has to assume a distribution. With no external stress applied the most reasonable assumption to make is that the tetragonal axis is found with equal probability along all cube directions. With respect to domain size, however, it is possible to establish a typical value $\bar{d}$ from x-ray or microscope photographs. We are interested in velocity shifts, and the change in transit time is the directly measured quantity. When $\lambda \ll \bar{d}$ we find the following expression for the relative velocity change:

$$\frac{\Delta v}{v} \simeq v\,\frac{\bar{d}}{L}\sum_{n=1}^{N}\frac{1}{v_n} - 1\,, \tag{15}$$

where L is the length of the sample and v_n is the velocity in the nth domain. The total number of domains seen in the propagation direction is $N \approx L/\bar{d}$. Due to the condition $\lambda \ll \bar{d}$, we have assumed that the sound velocity is well defined in each domain.

Taking into account the fact that pressure may be used to suppress the c axis in one or two directions, we find different expressions for velocity changes under the experimental conditions discussed in Secs. III and IV.

When $\lambda \gg \bar{d}$, a sound wave is sampling simultaneously all elastic constants which are effective in propagating the particular mode in question. While in the case just discussed the average had to be taken over the inverse velocities in various domains (or, more precisely, over the inverse square root of elastic constants), we now average over the elastic constants directly. In general these cases will be different, of course. The weight given to each elastic constant involved is simply the fractional number which says how much of the path is dominated by each elastic constant. For instance, take a longitudinal wave along a cube axis in the cubic phase. Below T_a one may take $\frac{2}{3}$ of the effective elastic constant to be C_{11}, $\frac{1}{3}$ to be C_{33}, i.e., $C_{eff} = \frac{2}{3}C_{11} + \frac{1}{3}C_{33}$, when we have assumed that the c axis occurs with equal probability along the three axes. When a pressure is put on, this will change the relative weights since the c axis may be suppressed in one or two directions depending on the way in which pressure is applied. Some cases of interest are listed in Table I.

E. Interaction with Domain Walls

We now turn our attention to an even more serious problem related to wave propagation in a domain structure. This is the contribution to the effective

elastic constants made by the domain walls. In our opinion this has lead to a serious shortcoming of the data analysis conducted in Refs. 12, 23, and 24. The problem has been mentioned in Refs. 12 and 23; however, no attempts were made to estimate the influence of these effects on the data.

The main influence of the domain walls on the sound velocity will be through strain-induced wall motion with subsequent relaxation towards equilibrium. This is a loss mechanism, and as such has the effect of slowing down the wave motion. If we assume a characteristic time τ for this relaxation process, then a general relation between the associated attenuation α_d, velocity v, velocity change Δv_d, angular wave frequency ω, and τ is (to first order in Δv_d)

$$\alpha_d = \frac{\Delta v_d \omega}{v^2} \frac{\omega\tau}{1+\omega^2\tau^2} . \tag{16}$$

v here corresponds to "high-frequency" wave propagation ($\omega\tau \gg 1$) which occurs close to T_a since τ usually takes for form $\tau = c_d/(T_a - T)$, where c_d = const.

If a plot is made of the maximum domain attenuation α_{max} (occurring at the temperature where $\omega\tau = 1$) vs ω, then the slope α_{max}/ω gives

$$\Delta v_d/v = 2v(\alpha_{max}/\omega) . \tag{17}$$

The velocity change due to interaction with domain walls can then be found, and may be subtracted from the total change measured to give the net velocity change associated with the soft-mode transition. According to measurements which we shall discuss in Sec. IV, this correction is required when substantial attenuation is found in the low-temperature phase.

It is important to realize that the problem is *not* avoided by reducing the temperature to the range where the attenuation has more or less vanished ($\omega\tau \ll 1$). The velocity change which has taken place does not diminish again even if the domain attenuation becomes negligible at low temperatures. Apparently this point was not realized in the references quoted above.

Finally we would like to point out that the velocity change Δv_d due to domain wall interaction occurs at a temperature where all changes due to interaction with the order parameter have taken place. This is due to the fact that the corresponding relaxation times differ by about two orders of magnitude (see Sec. IV). The two velocity changes we have discussed, therefore, are simply additive, and the desired change due to interaction with the order parameter can be found as

$$\Delta v_{LK} = \Delta v_{tot} - \Delta v_d ,$$

where Δv_{tot} is the total velocity change measured and Δv_d is determined from attenuation measurements in a way just described. The subscript LK refers to the fact that the net result is the velocity change of the form predicted by Landau-Khalatnikov theory.[25]

III. EXPERIMENTAL

A. Samples

Experiments were carried out on three samples, to be labeled I, IIA, and IIIA, respectively, all of which were purchased from National Lead Co. where they had been grown by the Verneuil method. The samples were prepared from different boules.

From EPR linewidths it had previously been esti-

TABLE I. Formulas for velocity changes in monodomain and polydomain samples, without domain wall interaction. Index c refers to the cubic phase.

		$\Delta v/v_c$	
$\vec{q}\parallel$	C^c	Monodomain	Polydomain random distribution assumed
[100]	C_{11}^c	$\frac{1}{2}(\Delta C_{11}/C^c)$	
			$\frac{1}{6}\frac{2\Delta C_{11}+\Delta C_{33}}{C^c}$
[001]	C_{11}^c	$\frac{1}{2}(\Delta C_{33}/C^c)$	
[110]	$\frac{1}{2}(C_{11}^c+C_{12}^c+2C_{44}^c)$	$\frac{1}{4}\frac{\Delta C_{11}+\Delta C_{12}}{C^c}$	
			$\frac{1}{12}\frac{2\Delta C_{11}+\Delta C_{33}+\Delta C_{12}+2\Delta C_{13}+4\Delta C_{44}}{C^c}$
[011]	$\frac{1}{2}(C_{11}^c+C_{12}^c+2C_{44}^c)$	$\frac{1}{4}\frac{\frac{1}{2}\Delta C_{11}+\frac{1}{2}\Delta C_{33}+\Delta C_{13}+2\Delta C_{44}}{C^c}$	

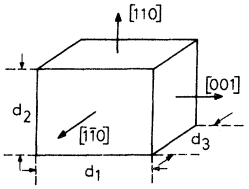

Sample	d_1 (mm)	d_2 (mm)	d_3 (mm)
I	9.56	4.70	4.73
IIA	2.59	4.95	5.07
IIIA	3.20	5.05	5.08

FIG. 2. Orientation and dimensions of samples used in the present work.

mated that the average internal stress was of the order of 10^8 dyn/cm^2 in similar samples. However, the samples used for ultrasonic measurements were very carefully cut and internal stress is likely to have been lower here. Dimensions and orientation of symmetry axes are given in Fig. 2.

In the course of the pressure experiments a certain additional strain was induced in the samples. Samples I and IIA were therefore annealed by heating to 1510 °C in an Al_2O_3 oven in oxygen at atmospheric pressure, and subsequently cooled to room temperature over 5 days. This slow cooling was considered necessary in order to maintain a homogeneous temperature. The ultrasonic echo pattern was improved by this procedure. However, quantitative determination of the reduction in internal strain was not made.

In order to avoid strain-induced interference near the transition we found it necessary to reduce the ultrasonic path length in the samples to a minimum. This minimum was given by the requirement that pulse-echo separation be preserved to sufficient degree. Measurements of the temperature-dependent attenuation were made on the peak of the first pulse only. The limiting factor is then the rise time of the pulse. In order to have no overlap with the second pulse at the peak of the first pulse it is necessary to have a pulse-peak separation greater than the rise time of the rf pulse. The transit time could thus be reduced to 0.65 μsec when using a Matec 560 unit for the ultrasonic measurements. This means that samples as short as 2.5 mm could be used. The amount of phase distortion could thus be reduced by an order of magnitude compared to that of standard samples. It should be mentioned that Nava *et al.*[26] used 20-mm prisms, but their measurements were made well above the transition and do not concern us here. In most of the work quoted in Sec. II, where sample sizes were given, sample lengths of around 20 mm were used in measurements through the transition. Since all of these samples were obtained from the same source as ours, we conclude that our method should offer considerable improvements with regard to elimination of strain effects. We have found these improvements to be essential in obtaining reliable measurements. A second advantage is the fact that temperature homogeneity is more easily and readily obtained.

B. Temperature and Pressure

Pressure could be applied to the sample during all measurements. The sample was located at the bottom of a stainless-steel tube with windows for attachment of electrodes, thermometer, and delay line. A piston could be pressed from above against the sample. The method used in applying biaxial (or planar) pressure is illustrated in Fig. 3. The force was applied through a steel spring and could be determined accurately by reading the compression of the spring which was located in the top end of the tube, at room temperature. Particular care was taken to avoid damaging the sample and to assure homogeneous distribution of pressure by always placing an indium foil (thickness 0.1–0.3 mm) on surfaces where pressure was applied.

To reduce temperature gradients in the sample to a millidegree level a 4-mm Teflon pad (not shown in Fig. 3) was put between the upper steel piston P and bracket B_1.

The thermometers used in most measurements were 50-μ-diam copper-wire resistance thermometers. These were found to agree with published data[27] for good-quality copper resistors and thus had an absolute accuracy of ~0.1 K. The noise in the temperature sensing system was low enough to permit a resolution of a few mK.

Temperature control was achieved first by manual adjustment and later by automatic feedback control of the input current in the heater element located below the sample. The heater was wound on a copper rod, making thermal contact to the liquid-N_2 bath below the same holder. Temperature stability of 0.01 K was obtained in this manner.

The surrounding N_2 vapor would tend to produce small temperature fluctuations in the sample due to unstable convection currents. Therefore the

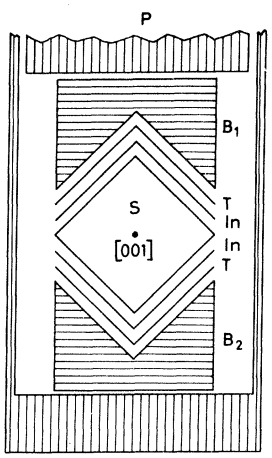

FIG. 3. Detail of sample mounting for application of biaxial pressure. The sample *S* is located in the center. Indium (In) and Teflon (*T*) sheets were inserted between brass brackets B_1 and B_2. Pressure is applied through the piston P.

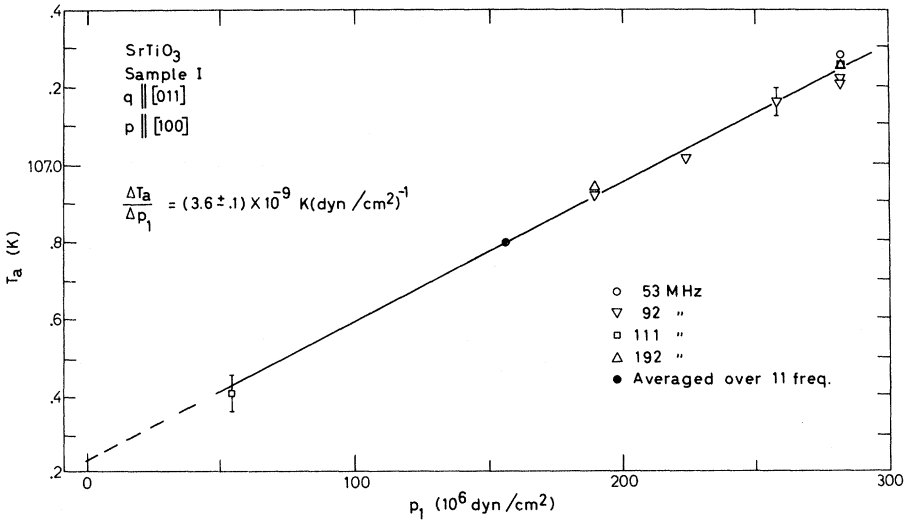

FIG. 4. Transition temperature $T_a(p_1)$ determined at various frequencies with uniaxial pressure $\vec{p} \perp \vec{q}$, and longitudinal waves.

sample holder was enclosed in a light polyester jacket that reduced convection currents near the sample to a minimum.

IV. RESULTS

The transition temperature T_a was identified as the temperature corresponding to the first attenuation peak appearing in a cool-down run. For a discussion of results in zero pressure, see Ref. 2. Results with uniaxial pressure along[28] [100] are given in Fig. 4. The change in transition temperature is seen to depend linearly on pressure as predicted by the theory in Sec. II. It should be noted that the transition temperature was defined by attenuation measurements over a wide range of frequencies. [The attenuation will be discussed separately later (see Figs. 9–11).] No discrepancies were found. From Fig. 4 one finds

$$\Delta T_a/\Delta p_1 = (3.6 \pm 0.1) \times 10^{-9}\ \text{K/dyn cm}^{-2}\ .$$

In Fig. 5 the corresponding results for biaxial pressure along [110] and [1$\bar{1}$0] are given. This stress was intended to make [001] the c axis for the whole crystal (monodomain). The result is again a linear dependence of T_a on pressure, as given by the constant ratio: $\Delta T_a/\Delta p_{1,2} = (9.2 \pm 0.3) \times 10^{-9}$ K/dyn cm^{-2}. We discuss the significance of these numbers below.

Figure 6 shows a series of attenuation measurements at constant frequency and different pressures

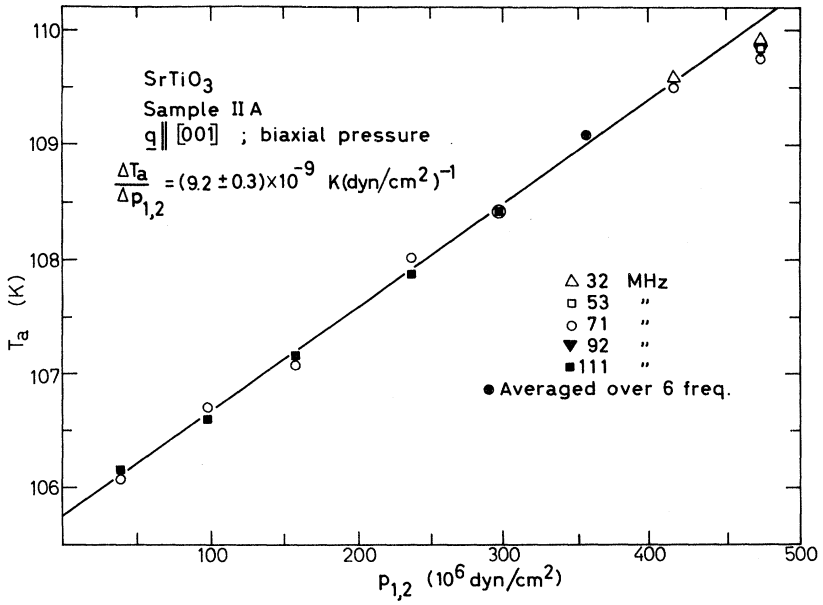

FIG. 5. Transition temperature $T_a(p_{1,2})$ with biaxial pressure $\vec{p} \perp \vec{q} \parallel$ [001] and longitudinal waves.

applied as in Fig. 5. Notice the improved quality of the sample as reflected in the higher attenuation peak and increased separation from domain-induced attenuation at high pressures.

Figure 7 illustrates the longitudinal velocity change observed with biaxial pressure applied as in Figs. 5 and 6, but on a sample of apparently lower quality. The critical-velocity minimum obtained in the best sample has been given elsewhere[3] and is shown in Fig. 13. In the present context we are interested mainly in the over-all shift in velocity. The method of measurement by which Fig. 7 was obtained (pulse-superposition technique) was more accurate than the direct delay-time measurements in Ref. 3. In spite of the poorer sample, the measurements in Fig. 7 therefore provide a better determination of the velocity *shift* and will be used in the calculations below. Since the domain scattering (lower peak) was not completely removed in the present case, the correction term associated with this scattering is taken into account in the numerical analysis. The lower curve in Fig. 7 illustrates the attenuation in the transition region. The upper peak is ascribed to critical scattering as discussed before.[2,3] The over-all shift in velocity in Fig. 7 is $-(1.65\pm0.07)\times10^{-2}$. After subtraction of domain contribution the net change is $-(1.47\pm0.07)\times10^{-2}$. Due to the applied stress, the c axis is, in this case, along the propagation direction, the elastic constant is C_{33}, and the shift $\Delta C_{33}=B_1^2F_3$ is determined. From the velocity shift we immediately determine the in-

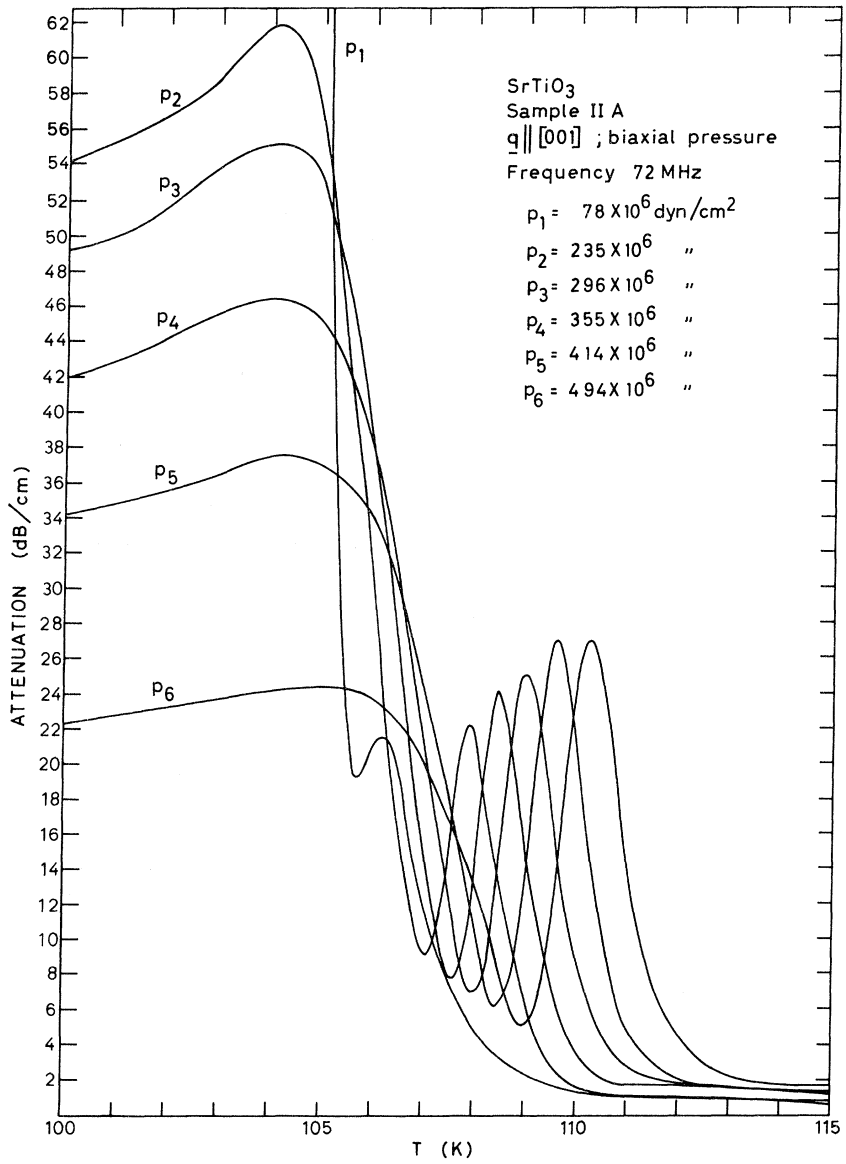

FIG. 6. Attenuation of longitudinal waves under biaxial pressure. Attenuation in the domain structure is strongly reduced by increasing pressure from P_1 to P_6. The absorption peak at T_a is increased and resolved from the domain attenuation by high pressures.

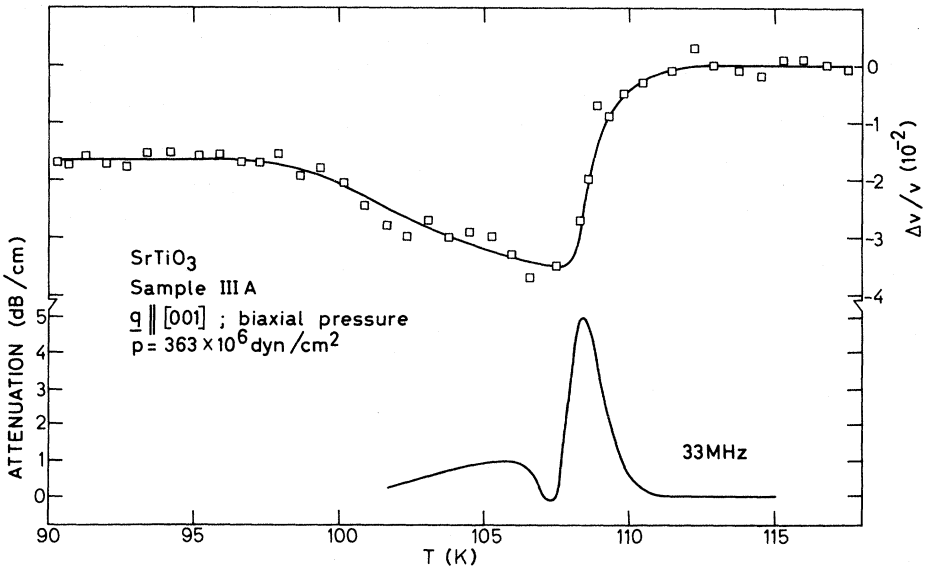

FIG. 7. Velocity measurements with longitudinal sound at 10 MHz and high biaxial pressure, upper curve. Attenuation measurements at 33 MHz, lower curve.

teraction parameter $B_1 = 1.87\times10^{27}$ erg/cm^5, using Eq. (14) for F_3 and taking $\rho_r = 0.895$ g/cm^3. The quantities Q, $\omega_{1,2}$, and ω_3 are assumed to have the same temperature dependence. They were determined at 77 K from existing data: $Q = 5.2\times10^{-10}$ cm, calculated from Ref. 13; $\omega_{1,2} = 2.20\times10^{12}$ sec^{-1}; and $\omega_3 = 6.60\times10^{12}$ sec^{-1} from Ref. 7. The lattice constant $a_0 = 3.90\times10^{-8}$ cm was taken from Lytle[29] and elastic constants above T_a from Ref. 22. For later use we also quote the numerical value of

$$\frac{dK}{dT} = \rho_r \frac{d\omega_c^2}{dT} = 3.98\times10^{23}\ \text{g/sec}^2\,\text{K}\,\text{cm}^3\,,$$

which is found from measurements[30,31] of the soft-mode frequency ω_c above T_a.

Using Eq. (8a) the parameter B_2 can now be calculated since $\Delta T_a/\Delta p_1$ and $\Delta T_a/p_{1,2}$ are given above. The two values for B_2 obtained are not in agreement. The first result leads to $B_2 = -0.71\times10^{27}$ erg/cm^5, while the second gives $B_2 = -1.08\times10^{27}$ erg/cm^5. Biaxial pressure produces a monodomain crystal, and the second result therefore must be preferred over the first one. Also it turns out that the lower value of B_2 would correspond to a negative change of T_a with hydrostatic pressure, contrary to observation.[11] We conclude that the difference must be due to domain influence in the uniaxial case. We discuss these problems further in Sec. V.

In Fig. 8 velocity measurements with longitudinal

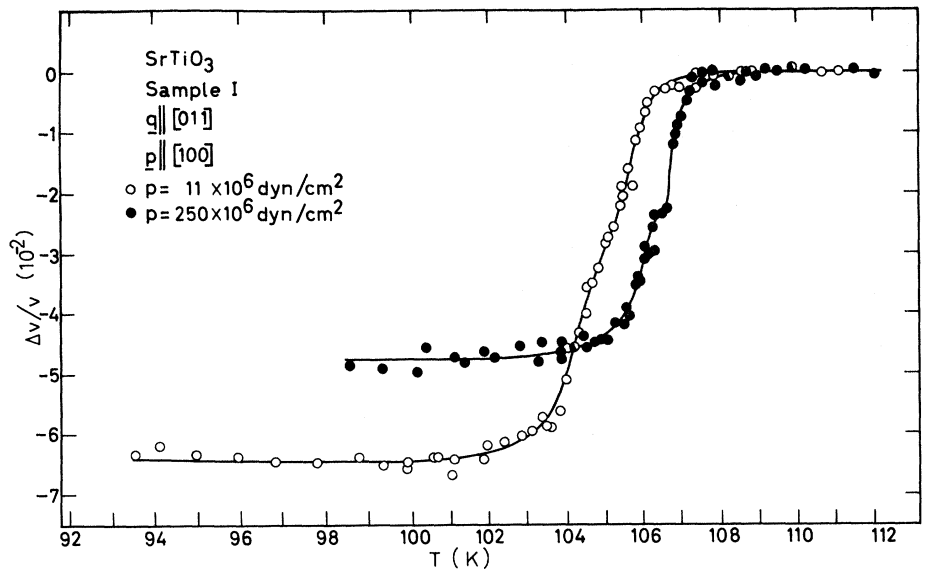

FIG. 8. Change of longitudinal velocity at 10 MHz with $\vec{q} \parallel [110]$ at two pressures. Increased pressure reduces the velocity change by suppressing domains. The curves are shifted along the T axis due to the pressure dependence of T_a.

waves along [011] are given for two different uniaxial pressures applied along [100]. Although not all ⟨110⟩ directions are pure-mode directions below T_a, calculations show that particle displacement may be only about 0.5° off the propagation direction, and therefore to a good approximation may be treated as a longitudinal motion. These remarks pertain to domains with the c axis at 45° with the propagation direction, which is the situation expected with uniaxial pressure along a cube axis normal to the wave vector q.

The removal of domains with the c axis along the direction of pressurization reduces the number of domain walls, and consequently the ultrasonic wave is less affected by domains at high pressure. This is seen experimentally as a very strong reduction in domain scattering and a significant reduction in the velocity shift. However, in order to analyze the velocity shifts for this propagation direction we first study further the domain effects. These are most easily revealed by attenuation measurements.

A notable feature of the ultrasonic attenuation below T_a is the frequency dependence of the domain scattering. This feature is illustrated in Fig. 9. The peak occurring at the lowest temperature is shifted with frequency. Its height is also frequency dependent. We associate the shift with a relaxational-loss mechanism due to domain wall motion of the type discussed in Sec. II. Expecting a temperature-dependent relaxation time τ of the form $\tau = c_d/(T_a - T)$, the peak position is plotted vs frequency in Fig. 10; $\Delta T_1 = T_a - T_1$ is linear, with $c_d = 1.63 \times 10^{-9}$ K sec which is about two orders of magnitude larger than the corresponding result for

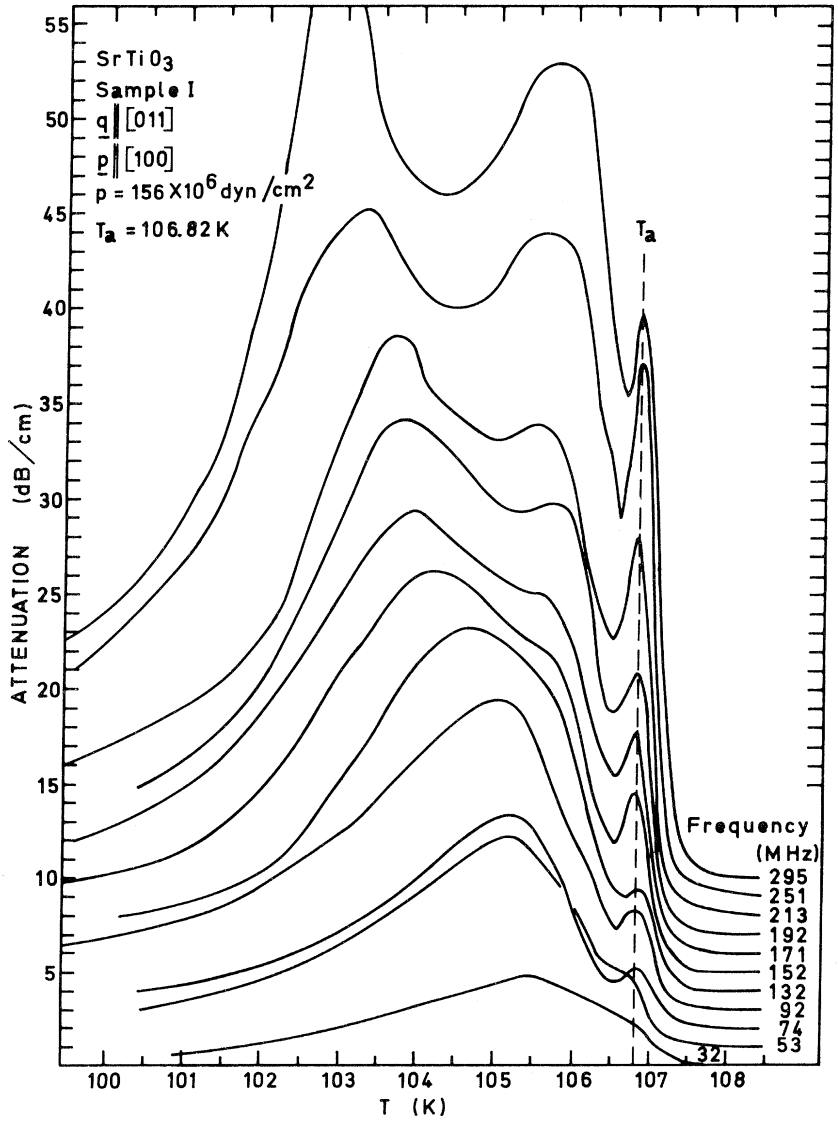

FIG. 9. Longitudinal attenuation with $\vec{q} \parallel [011]$ at moderate pressure $\vec{p} \perp \vec{q}$ measured at 11 frequencies.

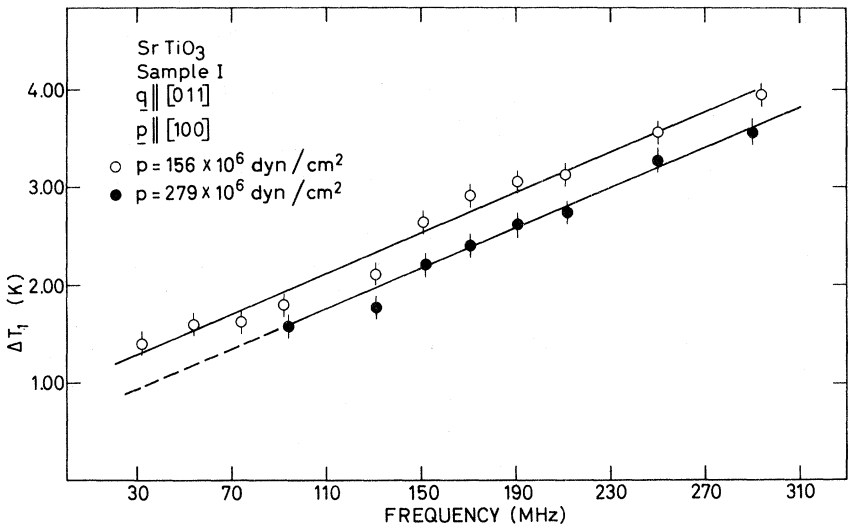

FIG. 10. The difference $\Delta T_1 = T_a - T_1$ plotted vs frequency from Fig. 9. T_1 refers to the temperatures at which the low-temperature peaks in Fig. 9 occur.

the relaxation time[20] of the order parameter. The test is carried out at two pressures; both lines have the same slope, indicating that the relaxation time is independent of pressure, as seems indeed reasonable to expect. As a second test we plot the attenuation maximum vs frequency in Fig. 11. A linear relation is found from 30 to 250 MHz. The scatter of low-frequency points is due to an unexplained middle peak which is superimposed here. The data plotted in Fig. 11 refer to the low-temperature maxima in Fig. 9.

One might reasonably attempt to ascribe the frequency-shifted peak to a matching between ultrasonic wavelength and a typical domain size $\bar{d}$. However, from microscope observation we find $\bar{d} \simeq 30-50\ \mu$ which is much smaller than typical wavelengths, making such an interpretation impossible. Furthermore, the frequency shift would require the domain size to diverge as $(T_a - T)^{-1}$, while observations show no such change to take place.

The plot of α_{max} vs frequency in Fig. 11 allows an accurate estimate of the velocity change associated with the domain wall motion alone according to Eq. (17) given in Sec. II. No velocity data were taken in connection with the attenuation measurements shown in Fig. 11; we present these data only to demonstrate how well the relation $\alpha_{max}/\omega =$ con-

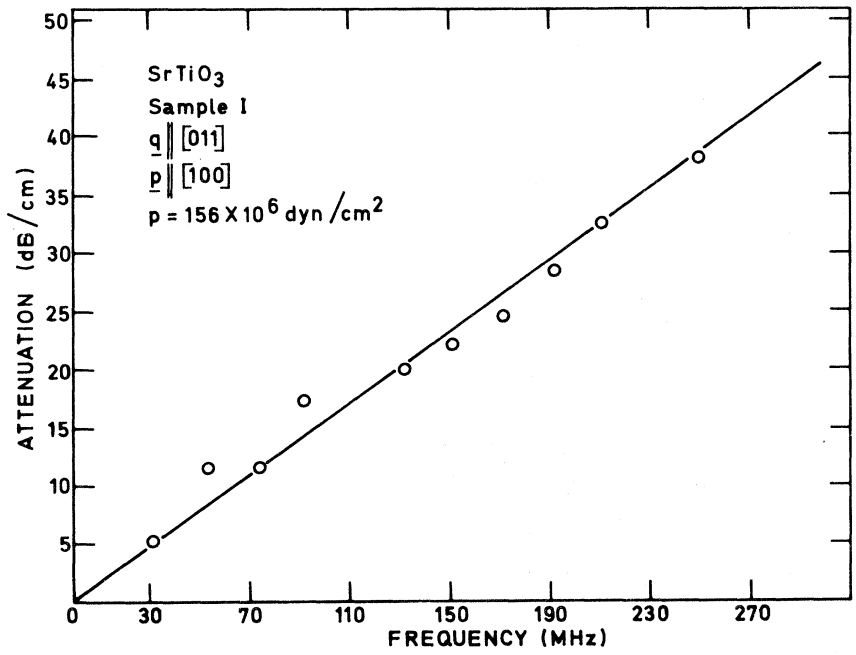

FIG. 11. Attenuation at the low-temperature peaks of Fig. 9 vs frequency.

TABLE II. Determination of velocity changes with $\vec{q} \| [011]$, normal to the pressure p.

Pressure p (10^6 dyn/cm^2)	Measured $\Delta v/v_c$ (10^{-2})	Domain attenuation α_{max} (dB/cm)	Frequency (MHz)	Velocity change due to $\Delta v_d/v$ (10^{-2})	Net change $(\Delta v/v_c)_{LK}$ (10^{-2})
11	−6.48	16	31.5	−3.05	−3.4
78	−5.39	8.5	32.5	−1.57	−3.8
		16.6	72	−1.39	−4.0
157	−4.86	...	...	...	...
245	−4.77	0.4	33.5	−0.08	−4.7
		2.4	72	−0.20	−4.6

stant is followed over a wide frequency range. Once this fact is established this relation can be invoked even when analyzing data for one frequency at a time, and this is what we have done in analyzing the data of Fig. 8 and further data taken in the same series. Table II gives the results of such analysis of simultaneous measurements of velocity shifts and attenuation, including the data given in Fig. 8. Pressure is along the cube axis. All velocity shifts were measured at ~10 MHz.

From the data given in Table II one can make further analysis of the interaction parameters: First of all the corrected high-pressure data may be used to calculate ΔC_{44}. Using the appropriate formula from Table I and calculating the shifts ΔC_{11} and ΔC_{13} from Eqs. (13) and (14), we insert the corrected high-pressure result for $\Delta v/v_c$ given in Table II and Fig. 12 and find $\Delta C_{44} = -0.33 \times 10^{12}$ dyn/cm^3 which makes $|B_t| = 2.3 \times 10^{27}$ erg/cm^5. The sign of B_t is not determined here. Slonczewski and Thomas find it to be negative and determine $B_t = -2.51 \times 10^{27}$ erg/cm^5, which is in fair agreement with our value. To make a further test of the consistency of our results we calculate the velocity shift in a polydomain sample with $q \| [110]$ on the basis of the numerical values of all three interaction parameters determined above. Using the formula in Table I we find $\Delta v/v_c = -3.4 \times 10^{-2}$ which agrees very well with the corrected low-pressure result for $\Delta v/v_c$ in Table II and Fig. 12.

The coefficients found above can be put to an extremely sensitive test by making a prediction of dT_a/dp (hydrostatic pressure) since this quantity was shown in Eq. (8c) to be proportional to $B_1 + 2B_2 = B_1 - 2|B_2|$. We calculate

$$\frac{dT_a}{dp} = (0.55 \pm 0.15) \times 10^{-9} \text{ K/dyn cm}^{-2}.$$

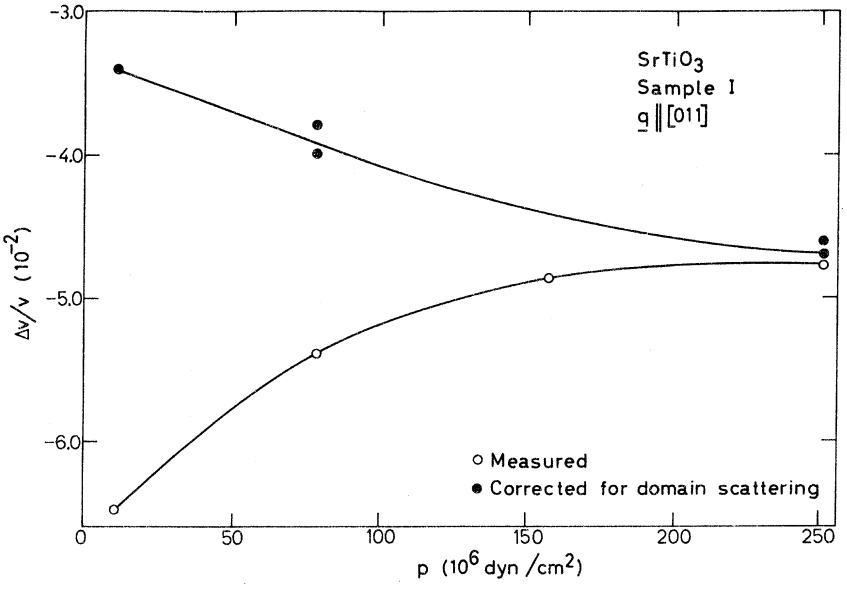

FIG. 12. Longitudinal velocity shifts vs pressure, determined with $\vec{q} \| [011]$, uniaxial pressure.

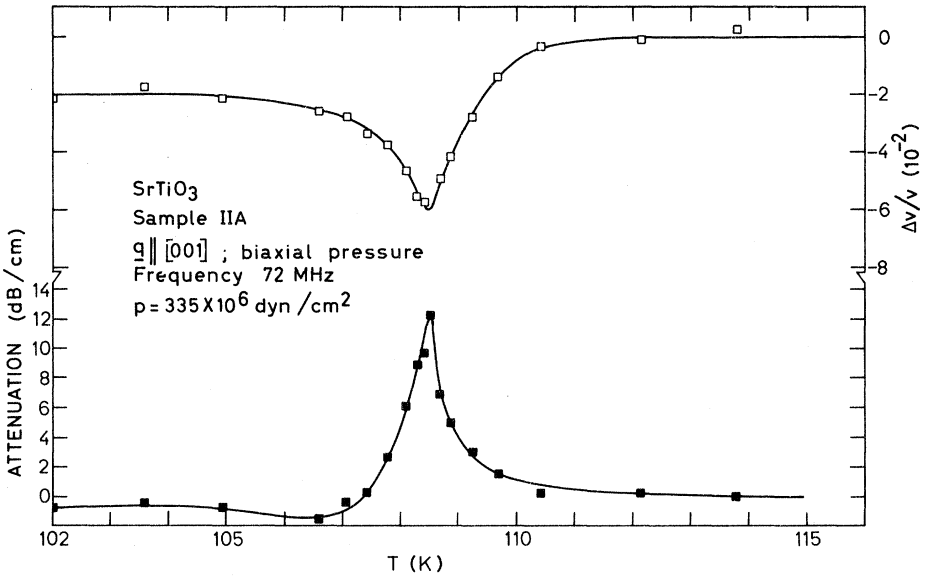

FIG. 13. Simultaneous measurements of velocity and attenuation at high biaxial pressure.

Further discussion is referred to Sec. V.

We conclude this section by giving some further results relating to the discussion of the nature of the transition. Figure 13 demonstrates simultaneous point-by-point measurements of velocity and attenuation, designed to answer in a qualitative way the question as to whether the interaction with the sound wave is critical or not. The answer is seen to be that both the LK mechanism and critical attenuation must be present. The velocity shift clearly indicates the presence of an interaction of the type predicted in the LK theory, superimposed on a minimum coinciding with the attenuation peak, signifying critical behavior as well. Straightforward calculations show that the LK peak should occur in a mK range below T_a at our frequencies, which means that it will be completely smeared out and cannot be correctly observed with the sample quality and temperature resolution of the present experiment. This estimate is based on measurement[20] of the order-parameter relaxation time.

The critical region, on the other hand, is much wider, as was suggested in Ref. 2 and later verified by different techniques.[13,14] Experiments show that the critical region is about 5 K wide on both sides of T_a, i.e., about a factor 10^3 wider than the LK dispersion region at our frequencies.

It is our experience that the removal of the domain structure by applying pressure is not successful unless extreme care is taken to obtain even distribution of the pressure. In Fig. 14 we have succeeded in completely removing the domain attenuation. In this case the temperature exponents may also be determined below T_a, which has not been done in domain-free crystals before. From Fig. 14 we find $\eta(T < T_a) = 1.52 \pm 0.10$ and $\eta(T > T_a) = 1.27 \pm 0.10$, where η is the exponent in the expression $\alpha \propto \omega^n |T_a - T|^{-\eta}$. We note that $\eta(T > T_a)$ determined here at high pressure is the same as we found[2] in zero pressure before.

V. DISCUSSION

The data may conveniently be discussed from two viewpoints: The most important test is to examine the internal consistency by use of the expressions developed in Sec. II. Also of interest is the comparison with published data, both ultrasonic and others. Although these are independent tests we shall not make an artificial distinction between them in the following.

Looking first at the data on the stress dependence of T_a, it was found that $\Delta T_a/\Delta p_{1,2} = 9.2 \times 10^{-9}$ K/dyn cm^{-2} (corresponding to $dT_a/dp_1 = 4.6 \times 10^{-9}$ K/dyn cm^{-2}), also implying that dT_a/dp_3 is about a factor of 2 lower than that given in Ref. 11. We remark that the measurements of Ref. 11 failed to identify the transition temperature itself, while this was always done in the present investigation. One may also notice that the present value is in far better agreement with the calculations of Slonczewski.[9] The prediction made here for $dT_a/dp = 0.55 \times 10^{-9}$ K/dyn cm^{-2} is about a factor 3 lower than given in Ref. 11. This does not appear disturbing in view of the foregoing remarks.

It is interesting to observe that analysis of more recent and accurate neutron data taken above T_a only[31] leads to interaction parameters $B_1 = 1.77 \times 10^{27}$ erg/cm^5 and $B_2 = -1.11 \times 10^{27}$ erg/cm^5, very close to our values. This agreement lends strong support to our results since the approximations used in fitting the theory given in Refs. 16

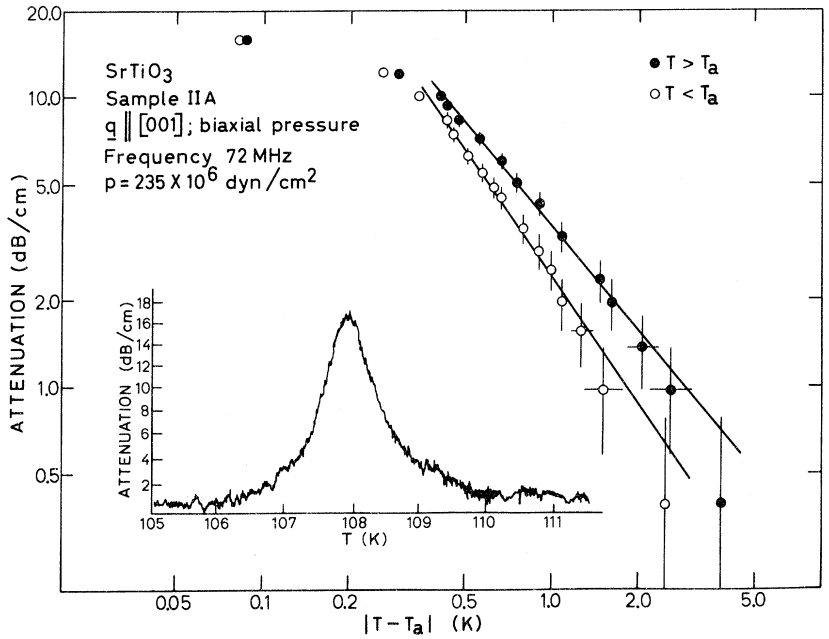

FIG. 14. Critical attenuation of longitudinal sound along [001]. Temperature exponents are determined from the plots to the right, both above and below T_a.

and 17 are quite good at high temperatures, while they tend to become inaccurate at low temperatures.[18] Earlier results for B_1 and B_2 found by Feder and Pytte[17] may therefore be regarded as more approximate since they insisted on fitting the data below T_a. In that case the agreement with experiments was somewhat lacking above T_a. The interaction constants of Ref. 31 give perfect agreement with our calculated value for dT_a/dp since this quantity is proportional to B_1+2B_2. Furthermore, the difference B_1-B_2 which enters in the left-hand side of Eq. (5) is also in perfect agreement.

In addition, Eq. (5) may be used to correlate the present data with the spontaneous-strain data of Alefeld.[32] From those data, and from Refs. 13 and 22, we calculate $C_e(e_3-e_1)/Q^2=3.1\times10^{27}$ erg/cm^5, while the left-hand side from our data is 2.9×10^{27} erg/cm^5. This again means that there is agreement within experimental accuracy.

Two qualitative requirements with regard to the ratios e_1/e_3 and B_2/B_1 may be stated here: Accepting the qualitative result of Ref. 11 that $dT_a/dp>0$ one sees from Eq. (8c) that one must have $B_2/B_1<-\frac{1}{2}$, which is satisfied by our value: $B_2/B_1=-0.58$. Equation (8c) also implies $e_1(0)+e_2(0)+e_3(0)<0$, or, since $e_1(0)=e_2(0)$, $e_1/e_3<-\frac{1}{2}$. The most likely ratio one can extract from Alefeld's data[32] gives e_1/e_3 slightly greater than $-\frac{1}{2}$; however, a ratio less than $-\frac{1}{2}$ is within the experimental error.

Thus, although Alefeld's data are not accurate enough to determine whether $e_1/e_3>-\frac{1}{2}$ or $e_1/e_3<-\frac{1}{2}$, which may require very high accuracy, they are capable of giving a reasonably accurate value of $e_3-e_1=e_3+|e_1|$.

On the other hand, if we use Eq. (6) to deduce e_1/e_3 from the present results and from Ref. 22, we find $e_1/e_3=-0.53$. Therefore, the second qualitative requirement stated above, $e_1/e_3<-\frac{1}{2}$, is also satisfied by the present data. Experimental results to test Eqs. (9)–(11) are not available at present, except Ref. 11 which we have already found incompatible with our results on a quantitative basis.

With regard to ultrasonic measurements[12,23,24] of the change in elastic constants we do not discuss these further here since they must be influenced by domain scattering and since corrections were not made to remove this contribution. In the present investigation domain effects were either removed by applying pressure, or the results were corrected for domain influence by use of Eq. (17).

We note, furthermore, that the present determination of ΔC_{44} is in very good agreement with two independent measurements[20,21] using Brillouin scattering. In the present work ΔC_{44} was extracted from sound-velocity measurements along [011] in a polydomain sample at high pressure. It involves both the use of B_1 and B_2, determined from measurements of ΔC_{33} and $dT_a/dp_{1,2}$, and the correction associated with domain scattering. This result, therefore, is quite reassuring both with regard to over-all consistency of measurements as well as the essential correctness of the model. In addition, when a prediction is made for the velocity shift along ⟨110⟩ in zero pressure, implying random-domain distribution, one finds $\Delta v/v_c$

$= 3.4 \times 10^{-2}$ which is again in very good agreement with measurements after correction for domain effects (Fig. 12). For $q \| \langle 111 \rangle$ we predict $\Delta v/v_c = -4.1 \times 10^{-2}$ for longitudinal waves. In Ref. 22 a change of -4.5×10^{-2} was measured.

In the foregoing discussion the biaxial-pressure result for $dT_a/dp_{1,2}$ was used throughout. The reason why the uniaxial-pressure result is incorrect, in our opinion, is the following: There is an intimate connection between the stress dependence of T_a and the spontaneous strains as shown in Eqs. (8a), (8b), (8c), and (11). Now, in a polydomain sample the c axes are pointing in three different directions, and by applying uniaxial pressure the sample cannot become monodomain. Thus Eq. (8b) is not in accord with the physical situation, and cannot be used to interpret the uniaxial case. By applying a biaxial pressure in the way described before this problem is resolved since the sample becomes monodomain.

Exactly the same type of difficulty will arise if one attempts to measure hydrostatic-pressure dependence or thermal expansion on polydomain samples. The latter experiment was done by Golding.[12] Using an expression similar to Eq. (8c) he deduced a numerical value for dT_a/dp. After correcting his Eq. (2) by a factor of 2 we find that his data give $dT_a/dp = 2.9 \times 10^{-9}$ K/dyn cm^{-2}, which is nearly a factor of 6 higher than our deduced value. Apart from the difficulties mentioned, the result may also be influenced by the fact that the measurements were made only in the transition region where later specific-heat measurements on the same material[33] showed a smeared-out jump and a general behavior which was found to be in disagreement with the results of Ref. 12. We suggest that the thermal-expansion experiments, as well as determination of dT_a/dp, should be carried out on monodomain samples.

We do not discuss the critical effects further here since we feel that a full theoretical clarification is needed with respect to the role played by the newly discovered[14] central mode[34] in $SrTiO_3$.

After completion of this manuscript we received a preprint by Rehwald[35] which deals with some of the questions discussed here. Our conclusions are not affected by the results of that investigation. As pointed out before, we believe the differences in the results can be ascribed to domain influence, which we have corrected for.

ACKNOWLEDGMENTS

The authors wish to express their gratitude to the Norwegian Council for Science and the Humanities (NAVF) for partial support of the present work. It is a pleasure also to acknowledge enlightening discussions with J. Feder, and to thank K. Motzfeldt and M. Steinmo for the aid given us in carrying out the time-consuming heat treatment of the specimens.

---

* Present address: Department of Physics, The Agricultural College of Norway, 1432 Vollebekk, Norway.

[1] *Proceedings of NATO Advanced Study Institute on Structural Phase Transitions and Soft Modes, Geilo, Norway*, 1971 edited by E. J. Samuelsen, E. Andersen, and J. Feder (Universitetsforlaget, Oslo, 1971).

[2] B. Berre, K. Fossheim, and K. A. Müller, Phys. Rev. Letters 23, 589 (1969).

[3] B. Berre and K. Fossheim, in Ref. 1.

[4] K. A. Müller, Helv. Phys. Acta 31, 173 (1958).

[5] H. Unoki and T. Sakudo, J. Phys. Soc. Japan 23, 546 (1967).

[6] K. A. Müller, W. Berlinger, and F. Waldner, Phys. Rev. Letters 21, 814 (1968).

[7] P. A. Fleury, J. F. Scott, and J. M. Worlock, Phys. Rev. Letters 21, 16 (1968).

[8] J. C. Slonczewski and H. Thomas, Phys. Rev. B 1, 3599 (1970).

[9] J. C. Slonczewski, Phys. Rev. B 2, 4646 (1970).

[10] H. Thomas and K. A. Müller, Phys. Rev. Letters 21, 1256 (1968).

[11] G. Sorge, G. Schmidt, E. Hegenbarth, and Ch. Frenzel, Phys. Status Solidi 37, K17 (1970); see also G. Sorge, E. Hegenbarth, and G. Schmidt, *ibid.* 37, 599 (1970); B. Pietrass and E. Hegenbarth, *ibid.* 34, K119 (1969).

[12] B. Golding, Phys. Rev. Letters 25, 1439 (1970).

[13] K. A. Müller and W. Berlinger, Phys. Rev. Letters 26, 13 (1971); K. A. Müller, in Ref. 1.

[14] T. Riste, E. J. Samuelsen, and K. Otnes, in Ref. 1; T. Riste, E. J. Samuelsen, K. Otnes, and J. Feder, Solid State Commun. 9, 1455 (1971).

[15] R. A. Ferrell, in *Proceedings of the International Symposium on Contemporary Physics, Trieste* 1968 (International Atomic Energy Agency, Vienna, 1969), p. 129.

[16] E. Pytte and J. Feder, Phys. Rev. 187, 1077 (1969).

[17] J. Feder and E. Pytte, Phys. Rev. B 1, 4803 (1970).

[18] J. Feder in Ref. 1.

[19] E. Pytte, Phys. Rev. B 1, 924 (1970).

[20] W. Kaiser and R. Zurek, Phys. Letters 23, 668 (1966); A. Lauberau and R. Zurek, Z. Naturforsch. 25a, 391 (1970).

[21] D. C. O'Shea, Bull. Am. Phys. Soc. 15, 383 (1970).

[22] R. O. Bell and G. Rupprecht, Phys. Rev. 129, 90 (1963).

[23] W. Rehwald, Solid State Commun. 8, 607 (1970).

[24] B. Lüthi and T. J. Moran, Phys. Rev. B 2, 1211 (1970).

[25] L. D. Landau and I. M. Khalatnikov, Dokl. Akad. Nauk SSSR 96, 496 (1954).

[26] R. Nava, R. Callarotti, H. Ceva, and A. Martinet, Phys. Letters 28A, 456 (1968); Phys. Rev. 188, 1456 (1969).

[27] T. M. Dauphine and H. Preston-Thomas, Rev. Sci. Instr. 25, 884 (1954).

[28] With regard to labeling of crystallographic directions, one should bear in mind that below T_a one has to

operate with two sets of indices: (i) those referring to the external faces of the crystal which are strictly correct only above T_a; and (ii) a set of indices referring to individual domains. Most of our indices refer to external faces. However, we also adhere to the convention that the c axis is along [001] in a single domain, as already explained in Sec II.

[29]F. W. Lytle, J. Appl. Phys. 35, 2212 (1964).
[30]R. A. Cowley, W. G. L. Buyers, and G. Dolling, Solid State Commun. 7, 181 (1967).
[31]K. Otnes, T. Riste, G. Shirane, and J. Feder, Solid State Commun. 9, 1103 (1971).
[32]B. Alefeld, Z. Physik 222, 155 (1969).
[33]P. R. Garnier, Phys. Letters 35A, 413 (1970).
[34]J. Feder, Solid State Commun. 9, 2021 (1971).
[35]W. Rehwald, Physik Kondensierten Materie (to be published).

PHYSICAL REVIEW B VOLUME 5, NUMBER 8 15 APRIL 1972

Effective Force Constant and Impurity Mode in the Low- and High-Frequency Limits

Bal K. Agrawal and P. N. Ram
Department of Physics, University of Allahabad, Allahabad, India
(Received 10 August 1971)

By employing an effective force constant introduced earlier in the framework of a rigid-ion model for the lattice dynamics we have discussed the asymptotic behavior of the high-frequency localized modes and the low-frequency resonance modes due to substitutional impurities in realistic cubic lattices. Simple expressions for the frequencies of these impurity modes and the linewidths of the resonance modes have been obtained. In the asymptotic description the motion of an impurity may be simulated by an Einstein oscillator which is vibrating in the rest of the host crystal assumed to be static. However, the dynamical correlation of the impurity with the other ions of the host lattice is found to be significant especially in the case of an impurity strongly coupled to the lattice. Numerical calculations have been made for CsI crystals doped with impurity ions of different species in the breathing-shell model. A good agreement between the theoretical and experimental results is observed. The values of the frequencies of the impurity modes and the linewidths of the resonant modes calculated in the asymptotic limits compare well with the experimental values. The discrepancy between the calculated and the experimental values in the majority of cases lie within 20%. In both the low- and high-frequency regions, the value of the effective force constant is seen to be independent of frequency. However, the value of the effective force constant in the high-frequency region is smaller in magnitude than that in the low-frequency region. Further, the value of the effective force constant does not depend on the kind of the ion in a unit cell in ionic crystal, i.e., the value is found to be practically the same whether we consider a positively charged impurity ion or a negatively charged impurity ion. The implication of these results is that one may employ a simple rigid-ion model for a realistic crystal lattice with central interactions for understanding the defect properties of solids in the low- and the very high-frequency regions.

I. INTRODUCTION

Quite striking changes in the vibrational properties of solids are observed when defects are introduced in them. Along with the alterations in the frequencies of the normal modes of vibrations of the crystal lattice, and in the pattern of the atomic displacements in the normal modes, there may appear localized or resonant modes. The localized modes are activated by a light impurity or a defect which is coupled to its neighboring atoms more strongly than a host atom. The frequencies of the localized or bound states lie in ranges forbidden to the normal modes of the pure host crystal. These are nonpropagating modes and are limited to a very small region around the impurity. Similarly, quasilocalized or resonant modes may also appear for a heavy impurity or a defect which is coupled weakly to its neighbors as compared to the host atoms. The frequencies of the resonant modes lie in the ranges of the frequencies allowed to the normal modes of the pure host crystal. These modes are characterized by a large vibrational amplitude of the defect or of those atoms with which it directly interacts. An increase in the density of states near the resonance frequency is observed which gives rise to resonance-type peaks in the frequency spectrum of the doped crystal. Further, these modes have finite lifetimes because they can decay into the band modes. The existence of the defect modes has been shown by a wide variety of experimental measurements. Anharmonic forces of the lattice affect significantly the properties of the impurity modes, e.g., their